

An analytical model for the identification of the threshold of stress intensity factor range for crack growth

Marzio Grasso (Corresponding Author)

School of Engineering and Technology
University of Hertfordshire
College Lane Campus
Hatfield, AL10 9AB
Email: m.grasso@herts.ac.uk
Telephone: +44 (0)170 728 4659.

Antonio De Iorio

Department of Industrial Engineering
Federico II University
Naples Italy 80125
Email: antonio.deiorio@unina.it
Telephone: +39 (0)81 768 2454

Yigeng Xu

School of Aerospace, Transport and Manufacturing
Cranfield University,
Cranfield, Bedfordshire MK43 0AL
Email: Yigeng.Xu@cranfield.ac.uk
T: +44 (0)1234 754406

George Haritos

School of Engineering and Technology
University of Hertfordshire
College Lane Campus
Hatfield, AL10 9AB
Email: G.Haritos@herts.ac.uk
Telephone: +44 (0)170 728 4239.

M. Mohin

School of Engineering and Technology
University of Hertfordshire
College Lane Campus
Hatfield, AL10 9AB
Email: m.a.mohin@herts.ac.uk

Yong K Chen,

School of Engineering and Technology
University of Hertfordshire
College Lane Campus
Hatfield, AL10 9AB
Email Y.K.Chen@herts.ac.uk
Tel. 44 01707 284280

Abstract

The value of the stress intensity factor (SIF) range threshold (ΔK_{th}) for fatigue crack growth (FCG) depends highly on its experimental identification. The identification and application of ΔK_{th} are not well established as its determination depends on various factors including experimental, numerical or analytical techniques used. A new analytical model which can fit the raw FCG experimental data is proposed. The analytical model proposed is suitable to fit with a high accuracy the experimental data and capable to estimate the threshold SIF range. The comparison between the threshold SIF range identified with the model proposed and those found in literature is also discussed. The ΔK_{th} identified is found to be quite accurate and consistent when compared to the literature with a maximum deviation of 5.61%. The accuracy with which the analytical model is able to fit the raw data is also briefly discussed.

Keywords: Damage tolerance, Fatigue thresholds, Long cracks, Threshold stress intensity factor, Linear Elastic Fracture Mechanics (LEFM), Fatigue crack growth.

Nomenclature

a = crack length (mm)

a_f = final value of the experimental crack length (mm)

B = specimen thickness (mm)

C, p, q, m = Forman's Constants

da/dN = crack growth rate (mm/Cycle)

h, τ, p, a_{th}, α, β, N_{th} = parameters of the model proposed in the present paper

K_c = fracture toughness (MPa√mm)

K_{MAX} = maximum value of the stress intensity factor (MPa√mm)

N = number of cycles

N_f = final value of the experimental crack life

Pmax = maximum value of the applied load (kN)

Pmin = minimum value of the applied load (kN)

R = load ratio

R2 = coefficient of determination

W = specimen width (mm)

γ = material parameter for the Klensil and Lucas model

ΔK = range of the stress intensity factor (MPa√mm)

ΔK_{th} = value of the stress intensity factor range threshold (MPa√mm)

ΔK_{th0} = value of the stress intensity factor range threshold for R=0 (MPa√mm)

1. Introduction

FCG threshold (ΔK_{th}) is one of the key parameters representing material resistance to fatigue crack growth (FCG). Newman referred to the Federal Aviation Administration (FAA) by mentioning that traditionally, threshold is used as a limit for the damage tolerance design (DTD) [1, 2]. The ΔK_{th} has been used over the past 40 years in numerous FCG models available in literature [3-18]. However, the identification of ΔK_{th} and its application in structures residual life prediction is not quite straightforward, as it varies both qualitatively and quantitatively due to various experimental, numerical and analytical methods and corresponding assumptions used [19]. Whilst FCG curves of physically small crack and microstructurally small crack have different shapes [20], FCG can be represented by the sigmoidal curve of the $\log(\Delta K) - \log\left(\frac{da}{dN}\right)$ for long cracks as shown in Fig 1 [21]. It depicts three regions, region I, region II and region III. Region I is taken as either very slow crack growth region or near threshold region since the SIF range of the sigmoidal curve in this region asymptotically approaches ΔK_{th} . The Paris Law [22] is normally applicable to the crack growth in Region 2. There are several models available to represent the whole sigmoidal curve covering all three regions. One of the models developed by NASA and represented by Forman and Mettu [10, 21] is given in Eq. (1).

$$\frac{da}{dN} = C \Delta K^m \frac{\left(1 - \frac{\Delta K_{th}}{\Delta K}\right)^p}{\left(1 - \frac{K_{max}}{K_C}\right)^q} \quad (1)$$

where, C , m , p and q are material constants, SIF range (ΔK) = maximum SIF (K_{max}) – minimum SIF (K_{min}), K_C = SIF at fracture and ΔK_{th} = SIF range at threshold.

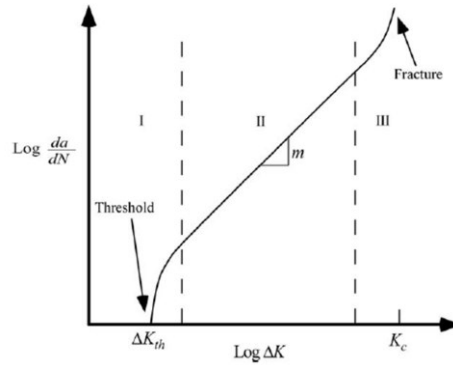


Fig. 1 Typical sigmoidal curve of fatigue crack growth [21]

Ideally, ΔK_{th} is the value of SIF range (ΔK) below which fatigue crack will not grow [21]. However, it has been shown [23] that cracks propagate even below the large-crack threshold measured by ASTM test procedure [1, 24]. Therefore, ΔK_{th} is also defined to be a value of ΔK at which crack growth rate (da/dN) is below 10^{-10} m/cycle [1, 25]. It is sometimes experimentally determined by extrapolation to $da/dN = 0$ from lower tail of the sigmoidal curve of raw data when linear-linear scale is considered [19]. Residual life of a structure can highly be influenced by a variation of the ΔK_{th} . As reported by Molent [18] and mentioned by Zerbst and Vormwald [19, 26], a variation in the threshold SIF range of 1 MPa m^{0.5} can result in a variation about 18% in the residual life. This also provides important insights into how relevant and reasonable it is to determine ΔK_{th} accurately in DTD approach.

There are several experimental methods available to determine ΔK_{th} . These are:

- Load reduction method (LRM);
- K_{max} constant method;
- Far-field cyclic compression method [19].

Load reduction method is standardised by ASTM 647 [24] or ISO 12108 [27]. The load is reduced stepwise to find ΔK_{th} in a pre-cracked specimen at a constant R . In K_{max} method the same stepwise reduction of the load range is followed but at the same time R is increased by maintaining the same maximum SIF value. The far-field compression method can be divided into three sub-methods including:

- Compression pre-cracking constant amplitude (CPCA);
- Compression pre-cracking load reduction (CPLR)
- Cyclic R curve method.

A detailed review of all these methods is given by Zerbst in [19].

The ΔK_{th} values obtained with the mentioned methods can however be quite different due to the different mechanisms involved. These mechanisms are related to the plasticity induced ahead of the crack tip as well as the conditions of the fracture surfaces. Comparatively lower threshold values have been found using the far-field cyclic compression method rather than using the load reduction method [1, 2, 28-30]. This is due to the fact that the far-field cyclic compression method is affected by the compressive yielding at the crack-starter notch and more “steady-state” constant amplitude data in near threshold regime is achieved with this method [29]. Crack surface roughness and grain size near the crack tip also influence the overall ΔK_{th} [1, 31]. In general, greater size of grains promotes roughness induced crack closure (RICC) and oxide-induced crack closure (OICC) is enhanced simultaneously [32]. The above phenomena increase the ΔK_{th} values when measured. Consequently, in LR Method crack-faces can produce rough-surface or fretting debris which contributes to the early crack closure and higher ΔK_{th} . The ΔK_{th} varies with mechanically short and long cracks. Linear-elastic fracture mechanics (LEFM) is normally only applicable in long cracks under small scale yielding conditions. Newman [33] has recently referred that ΔK_{th} is not valid in giga-cycle fatigue region for short cracks as there is no continuous crack propagation below $(da / dN) = 10^{-7} mm/cycle$, which is smaller than one lattice spacing per cycle [19]. In general terms, it is possible to find in literature [34] two different ΔK_{th} levels: microstructural threshold for short crack and mechanical threshold for long crack [35]. The difference is related to the advancement of a short crack at microstructural level and stable propagation of a longer crack having a plastic zone which covers several grains. Moreover, at low SIF the FCG rate is more sensitive to microstructure, load ratio and environment for long cracks [20]. However, there is a minimum value independent of R , which can be considered as material property and for this reason is called intrinsic threshold, also known as effective or true threshold [34]. Moreover, intrinsic threshold can be increased by the increase of stiffness and strength of the material [19, 36, 37]. Another important effect is related to the specimen geometry. ΔK_{th} seems to be lower in M(T) specimen than C(T) specimen for the same ΔK condition [38, 39]. The justification should be related to the geometrical constraint or $T - stress$, which is found to be lower in M(T) specimen ($T - stress < 0$), compared

to C(T) specimen ($T - stress > 0$) even though $T - stress$ has different effects (e.g. PICC) which might contradict this observation. However, the lowest stress triaxiality at the crack tip associated to the M(T) specimen, produces a much bigger plastic zone near the crack tip than the geometry with a high level of the constraint like the C(T) specimen [40].

Considering the fact that it is difficult to separate the extrinsic threshold from the intrinsic threshold using the crack growth data [34], the focus of this paper is to develop a model which can reliably predict the overall threshold of the material under certain loading conditions. In particular, since the model makes use of the raw data generated with a given specimen geometry under certain loading conditions, the analysis of the raw data includes both the load ratio and the T-stress effects. The value identified with the model can be an intrinsic or an extrinsic value depending on the testing conditions at which the data has been acquired.

As discussed above, the ΔK_{th} value usually decreases with the increase of R [41]. Two types of R-dependency have been reported in literature [34]. In some cases, ΔK_{th} decreases up-to a critical value of R then it becomes constant beyond that value [19]. In other cases, ΔK_{th} continues to decrease beyond the critical value of R [42]. Klensil and Lucas [3] used the following equation to identify ΔK_{th} in a steel alloy.

$$\Delta K_{th} = \Delta K_{th0}(1 - R)^\gamma \quad (2)$$

where, R is the stress ratio, ΔK_{th0} is the fatigue threshold value at $R = 0$ and γ is the material constant. However, other approaches [43] have been adopted like the one reported by Kwofie in which an equivalent stress approach based on R ratio is used to identify fatigue threshold value. In general, it has been recognised that crack closure is found to be the controlling factor in this case [18, 44]. For this reason, a different parameter has been introduced ΔK_{thr} , which is a FCG threshold value that depends on R and the crack length value. In literature the scatter in fatigue life was explained by the variation of ΔK_{thr} values [18]. Further methods to experimentally identify the threshold condition have been recently developed using plain fretting crack arrest analysis. The dispersion between long crack ΔK_{th} fretting estimations and conventional fatigue data was found to be less than 10% [45].

Due to the high variability of the ΔK_{th} values, the determination of the FCG threshold cannot be certain [19]. Although several models have been proposed to experimentally identify the threshold values, all of them suffer with issues related to the plasticity induced closure effects. For this reason, threshold values reported in

literature for the same material can vary in a wide range due to the different procedures that were followed. The aim of this paper is to present a new procedure to identify FCG threshold value for long crack which can overcome the problems related to the experimental procedures reported in literature. The analytical model proposed here makes use of FCG data obtained from K-increasing tests, which are used to derive the FCG properties of the material under the long crack condition, allowing to identify under the same testing conditions the three regions of the entire sigmoidal curve, from the threshold condition up to the final value of the crack length.

2. Test results for model development

Propagation models built on results obtained from a limited number of tests not only have a validity range closely linked to the particular experimentation carried out, but also are not suitable to fit all crack growth data with the same accuracy for the whole field of number of cycles for each test [46]. In order to overcome these drawbacks, several FCG data sets obtained with different materials, loading conditions and type of specimens have been collected from literature. These datasets have been used to verify the suitability of the model in fitting the experimental raw data as well as to identify the ΔK_{th} values of the materials at the corresponding R values. A short description of the datasets collected from literature is as follows.

Ghonem and Dore [47]

Ghonem and Dore [47] carried out tests at room temperature using M(T) specimens made of aluminium alloy 7075-T6 having a thickness of 3.175 mm. The crack direction was perpendicular to the rolling direction and the loading conditions are reported in Table 1. Sixty specimens were tested under each loading condition.

Table 1 - Loading conditions related to Ghonem&Dore tests.

	P_{max} (kN)	P_{min} (kN)	ΔP (kN)	R
Test I	22.79	13.68	9.11	0.6
Test II	22.25	11.13	11.12	0.5
Test III	15.19	6.08	9.11	0.4

Virkler et al. data [48]

The experimental activity reported by Virkler et al. [48] was aimed at determining which crack growth rate calculation method yields the least amount of error when the crack growth rate curve is integrated back to obtain the original ‘a’ versus ‘N’ curve data. Crack growth tests were carried out on 68 M(T) specimens, made of aluminium alloy 2024-T3 and having a thickness of 2.54 mm. All tests were conducted under the cyclic load with a maximum value of 5.25 kip/23.35 kN and a minimum load of 1.05 kip/4.67 kN at R=0.2.

Wu and Ni data [49]

The experimental work of Wu and Ni [49] was carried out on compact tension C(T) specimens made of aluminium alloy 2024-T351, having thickness B = 12 mm and width W = 50 mm. Tests were carried out with variable and constant amplitude loading. The two samples marked by the authors as CA1 and CA2 and composed of 30 and 10 specimens respectively, were tested at constant amplitude loadings reported in Table 2.

Table 2 - Loading conditions related to Wu&Ni tests.

	P_{max} (kN)	P_{min} (kN)	ΔP (kN)	R
CA1	4.5	0.9	3.6	0.2
CA2	6.118	3.882	2.236	0.63

3. Model implementation

The analysis of experimental data obtained from FCG test is quite complex due to the scatter nature in the raw data which is amplified by the derivation needed to compute the FCG rate. Several useful formulae to fit the experimental data with the aim of a better, smoother curve have been proposed and reported in literature. Among those, the use of a polynomial function to fit the raw data gives the possibility of obtaining a single numerical expression of the crack growth rate valid in the entire data range [46]. The choice of the most appropriate function can be made considering that the crack growth is exponential by nature. In mathematical terms an exponential correlation can be represented introducing logarithmic functions for the crack length [50-52]. This linear correlation ($\log(a)$ vs N) can be represented on a semi-logarithmic plane as a straight line. There are models proposed in literature which are developed adopting an exponential structure [52]. However, the trend identified using the experimental FCG data changes as the crack length approaches the failure condition. This consideration is supported by the presence of three different regions in the sigmoidal curve with each of

them following a different trend. On the basis of the aforementioned observations, the most suitable formula to fit the whole FCG experimental data points can be deduced by summing the individual effects of the different crack growth regions [53]. Therefore, the following model, on the basis of a trial and error method, could be established.

$$\mathbf{a}(\tau) = \mathbf{h} \cdot \tau^p + \mathbf{a}_{th} \cdot e^{\left(\frac{\tau^\alpha}{\beta - \tau^\alpha}\right)} \quad (3)$$

where α , β and p are three parameters to be determined by the least-square method. The procedure to derive the values corresponding to h and a_{th} is described in later parts of this paper. The proposed model makes use of a non-dimensional fatigue crack life, which makes it more general. Moreover the non-dimensional fatigue crack life allows decoupling the identification of the equation parameters, which are meant to be a material property, from the actual total life for the particular test. The non-dimensional fatigue life τ is defined as follows:

$$\tau = \frac{N + N_{th}}{N_f + N_{th}} \quad (4)$$

The parameter N_{th} , which is identified through best-fit curve together with three parameters (α , β and p) reported above, is related to the nucleation phase and hence to the threshold value. N_f is the final value of the experimental crack life, which is the number of cycles counted from the initial crack length up to the final failure of the specimen, whilst N is the generic value of the fatigue crack life.

Useful formulae can be derived for other parameters in Eq. (3) by considering some specific data points of the crack growth curve. At $N = N_f$, which corresponds to the last experimental data point of the test, the crack length is equal to the value of the crack length a_f in the corresponding last front just before the failure condition of the specimen. This gives:

$$\mathbf{h} = \mathbf{a}_f - \mathbf{a}_{th} \times e^{\left(\frac{1}{\beta - 1}\right)} \quad (5)$$

Similarly, considering the value of Eq. (3) at $N = 0$, which corresponds to the first experimental data point, the crack length is equal to the value of the crack length a_{th} corresponding to the starting point of the test. This gives:

$$a_{th} = \frac{a_{th} - a_f \times \left(\frac{N_{th}}{th+N_f}\right)^p}{e^{\left(\frac{\left(\frac{N_{th}}{N_f+N_{th}}\right)^\alpha}{\beta - \left(\frac{N_{th}}{N_f+N_{th}}\right)^\alpha}\right) - \left(\frac{N_{th}}{N_f+N_{th}}\right)^p \times e^{\left(\frac{1}{\beta-1}\right)}} \quad (6)$$

As already stated, the parameter N_{th} is related to the threshold condition and represents the number of cycles needed by the crack to reach the crack length corresponding to the threshold condition. From Eq. (3) the crack length in correspondence to the threshold condition is equal to the value of the a_{th} parameter in correspondence of $N = -N_{th}$.

Eq. (3) is a continuous differentiable function in the range $N_{th} < N < N_f$. It is therefore possible to derive the analytical expression of the crack growth rate $\left(\frac{da}{dN}\right)$ as a function of N . The function (Eq. (7)) can be used to represent the continuous propagation process from threshold region up to the final fast crack growth region.

$$da/dN(N) = \frac{h \left(\frac{N+N_{th}}{N_f+N_{th}}\right)^p}{N+N_{th}} + a_{th} \left(\frac{\left(\frac{N+N_{th}}{N_f+N_{th}}\right)^\alpha}{(N+N_{th}) \left(\beta - \left(\frac{N+N_{th}}{N_f+N_{th}}\right)^\alpha\right)} + \frac{\left(\left(\frac{N+N_{th}}{N_f+N_{th}}\right)^\alpha\right)^2}{\left(\beta - \left(\frac{N+N_{th}}{N_f+N_{th}}\right)^\alpha\right)^2 (N+N_{th})} \right) e^{\frac{\left(\frac{N+N_{th}}{N_f+N_{th}}\right)^\alpha}{\beta - \left(\frac{N+N_{th}}{N_f+N_{th}}\right)^\alpha}} \quad (7)$$

The parameters in the crack growth rate function are identified by means of the linear regression using the FCG raw data. The analytical expression of the crack growth rate is equal to zero at $N = -N_{th}$ according to the assumption that the crack length at this value corresponds to the threshold condition.

The procedure of applying the formulae of the analytical model to derive the threshold SIF range is as follows:

- The experimental raw data of crack length versus number of cycles are fitted using Eq. (3). The method adopted for the fitting is the linear regression to identify the four parameters of N_0 , α , β and p and minimize the error. In earlier paper [53] the model here presented was adopted to assess the accuracy in fitting the raw data produced during FCG tests. In the same paper [53], the normal distribution of the residuals as well as the distribution of the equation parameters have been included. In the present paper the discussion is focused on the identification of the threshold SIF range through the use of the analytical model proposed by the Authors.

- After the identification of the four parameters N_0 , α , β and p the values of the other two parameters h and a_{th} can be computed.
- To identify the six parameters used in the analytical formula representing the crack length as a function of the fatigue crack life as well as the corresponding function of the crack growth rate.
- A vector in the range $[-N_{th}; N_f]$ composed of n values is generated. For each value of the vector defined above, the corresponding values of the crack length and the crack growth rate are determined using Eqs. (3) and (7). The crack length values derived from Eq. (3) are used to deduce the SIF range values by means of the expressions in accordance with the international standards. It means that the method requires the knowledge of the closed form of the SIF for the tested specimen. In this paper the expressions reported by the ASTM E647 [24] have been used to compute the SIF values.
- The value of the crack length corresponding to $N = -N_{th}$ is used to derive the value of the threshold SIF range which corresponds to a crack growth rate equal to zero.

The procedure described above has been implemented in a Matlab code to identify the FCG curves and the ΔK_{th} values using the datasets produced by Ghonem and Dore, Virkler and Wu and Ni. The detailed discussion about the capability of the model to properly fit the datasets used in this paper is given in an earlier paper [53]. Fig. 2 shows some examples of fitting results with the experimental points related to set I produced by Ghonem and Dore.

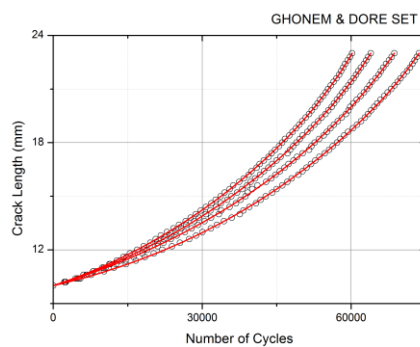


Fig. 2 Four crack growth data from Ghonem and Dore dataset [47] - raw data (dots) analytical model (in lines)

Moreover, normality of the residuals obtained from each curve has been verified by the χ^2 normality tests and the corresponding residuals frequency histograms have also been evaluated. In Fig. 3, the means of residuals for

Ghonem and Dore set I and set III are shown as an example to highlight that the mean value is equal to zero [53].

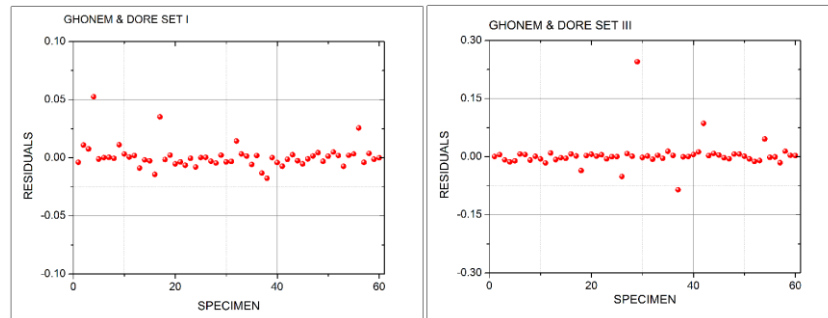


Fig. 3 Mean of residuals obtained by fitting Ghonem and Dore set I (left) and Ghonem and Dore set III (right)

A further version of the Matlab code, which was already implemented for the fitting curves, was developed further in order to identify the values of the FCG rate as well as the SIF range values. In particular, the SIF values in correspondence of $N = -N_{th}$ for each curve of all datasets have been computed in order to estimate the threshold values and compare these with those reported in literature.

4. Results and analyses

The interpolation of the raw experimental data represents the first step of the analysis. The suitability of the equation for fitting the data has been summarised in the above section. In particular, the raw data fitting has an average value of the R^2 equal to 0.9998 for all dataset [53]. The values of the parameters identified for each dataset are shown in Table 3

Table 3 - Parameter values for the five datasets

	α	β	N_{th}	p	h	a_{th}	ΔK_{th} MPav/m
Ghonem&Dore-Set No. 1	1.91	1.34	914314	4.40	6.75	0.81	1.42
Ghonem&Dore-Set No. 2	1.69	1.33	695502	3.43	6.33	0.72	1.63
Ghonem&Dore-Set No. 3	4.73	1.53	1635716	4.58	6.38	1.57	1.90
Virkler	2.93	1.28	2211197	6.59	19.84	0.75	2.79
Wu&Ni	58.04	1.85	842999	6.45	21.25	3.65	3.61

The values reported in Table 3 have been computed as an average of the values identified over the total number of tests for each dataset.

The crack length as a function of the number of cycles derived in the range $[-N_{th}; N_f]$ is shown for each data set in Fig. 4. In particular, the curve fitting related to the three datasets produced by Ghonem and Dore is shown

in the top row of the Fig. 4 (Set I - Set II - Set III), the curves related to the dataset produce by Virkler and the curves related to the datasets produced by Wu-Ni are shown bottom row of the Fig. 4. In each dataset all the fitting curves tend to the same asymptotic value as the number of cycles approaches $-N_{th}$. Although, the values are different between the various datasets. . In order to make possible the comparison between the experimental data points and the curves identified with the analytical model, the logarithmic plot of the horizontal axis, which is the number of cycles, has been used. The logarithmic scale is only used for the sake of clarity of the graph whilst the equations adopted are not affected by this choice.

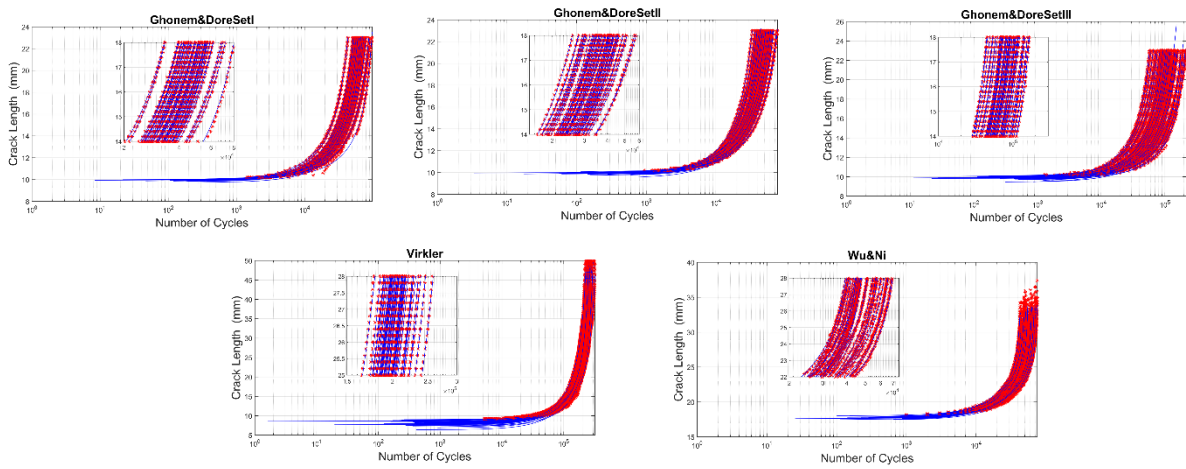


Fig. 4 Comparison of raw (dots) and analytical (lines) crack length vs number of cycle for the 5 datasets

In order to draw the FCG curve for the entire range, it is necessary to derive the crack growth rate together with the SIF range for the corresponding values. The curves shown in Fig. 5 correspond to all experimental data of the data sets considered in this paper. These graphs show clearly that the gradient approaching $N = -N_{th}$ is equal to zero, which reflects the asymptotic behaviour in the $a-N$ curves. As a consequence the FCG rate, as expected, approaches zero.

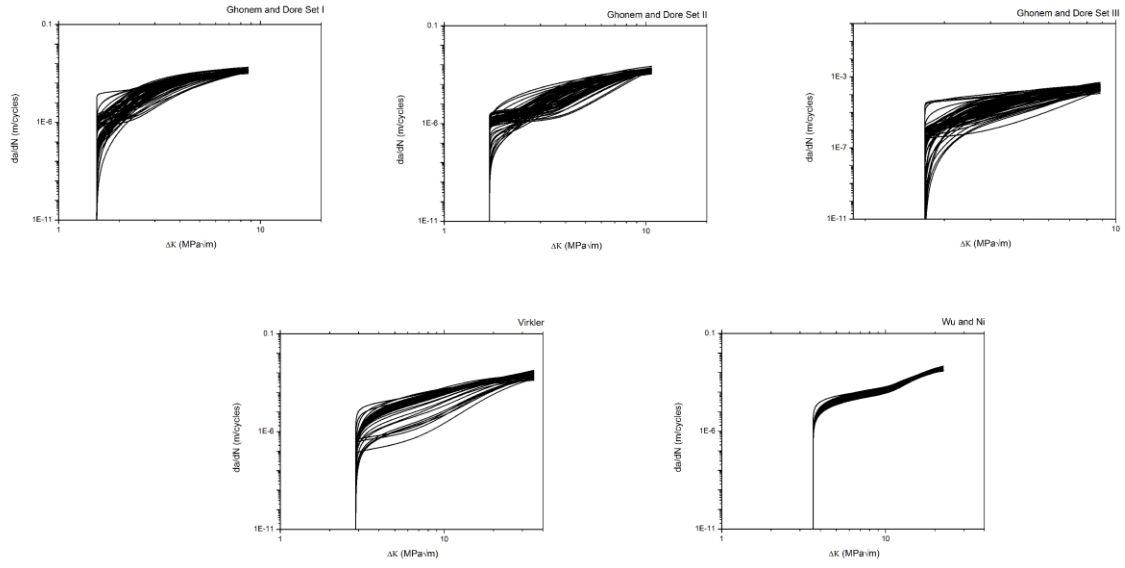


Fig. 5 FCG curve for the five datasets.

This observation can be used to extrapolate the crack growth curve from the lower part. The value of the threshold SIF range is found where $N = -N_{th}$. By means of Eq. (3), the value of the crack length at $N = -N_{th}$ can be derived. In Fig. 6, the values of the threshold SIF predicted by the model for each curve of the five data sets analysed in this paper are shown together with the corresponding values gathered from literature [44].

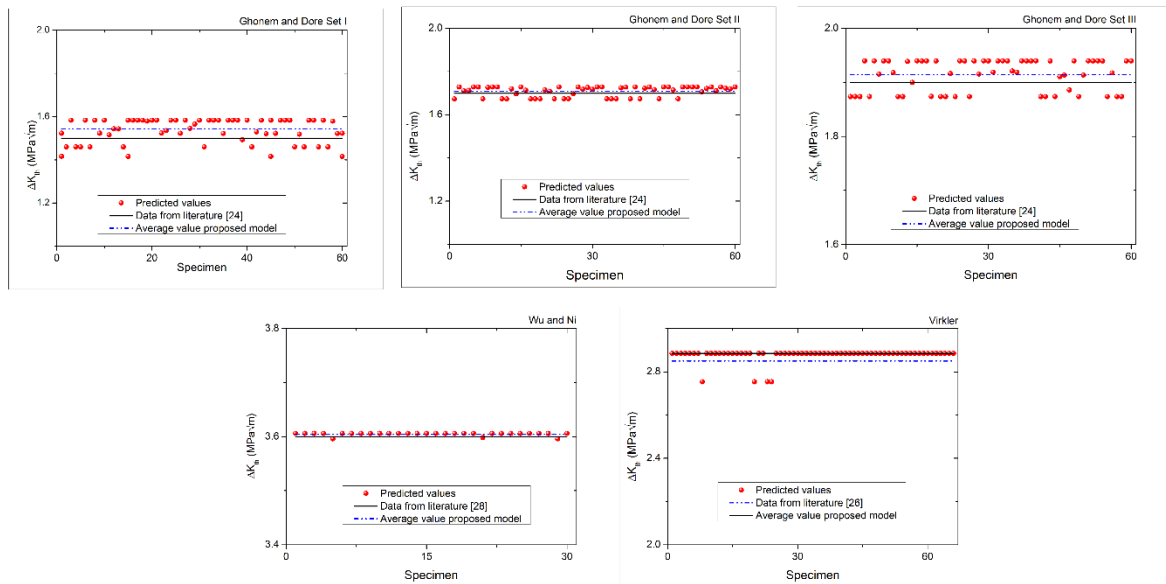


Fig. 6 Threshold SIF range for the five datasets.

5. Discussions

The crack length vs number of cycle curves found from the model correlate well with the raw data points. To relate the parameter values obtained by means of best-fit to the testing conditions, the contour plots shown in Fig. 7 have been created. The contour plots can be used to identify the range in which the optimal values of the model parameters should be identified by means of the best-fit of the experimental raw data in terms of crack length versus number of cycles. Nevertheless, the possibility of correlating the model parameters with the loading conditions by means of analytical expression can be adopted. This would allow to either reduce the number of parameters that can be identified through best-fit or to identify the FCG curve for a given material under certain loading conditions, which are usually defined in terms of maximum load and load ratio. For this reason the correlations between the 6 parameters of the proposed model and the maximum load P_{max} , and the load ratio R have been investigated using the values obtained from the fitting analysis carried out with the datasets found in literature and already discussed in this paper. In the following figures (Fig. 7), P_{max} is defined as the maximum value of the applied load in each cycle.

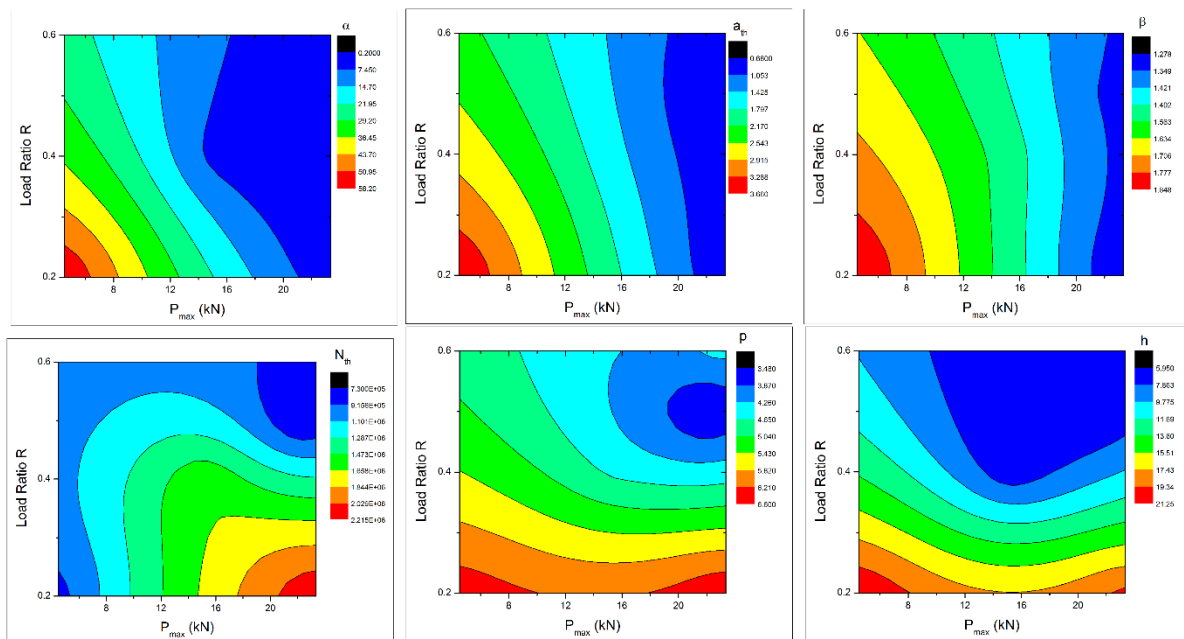


Fig. 7 - Contour plot of the model parameter average values in function of the loading conditions.

The two parameters α , β and a_{th} depend on the load ratio for low values of the maximum applied load only. At higher values of the maximum applied load the range of the above parameters is the same whatever the load ratio is, which means they are independent of the load ratio. Moreover, their values decrease as the values of R

and P_{max} increase. A different trend can be observed from referring to the model parameters of N_{th} , p and h . The combined effect of the load ratio and the maximum applied load is always present for the investigated range values of the loading conditions. In addition, the values of the two parameters p and h decrease as the values of R and P_{max} increase, whilst for N_{th} the trend is opposite with regard to P_{max} . In the graphs shown in Fig. 8 the correlations identified between the model parameters and the loading conditions are shown. In some cases the combination of more than one parameter has been considered.

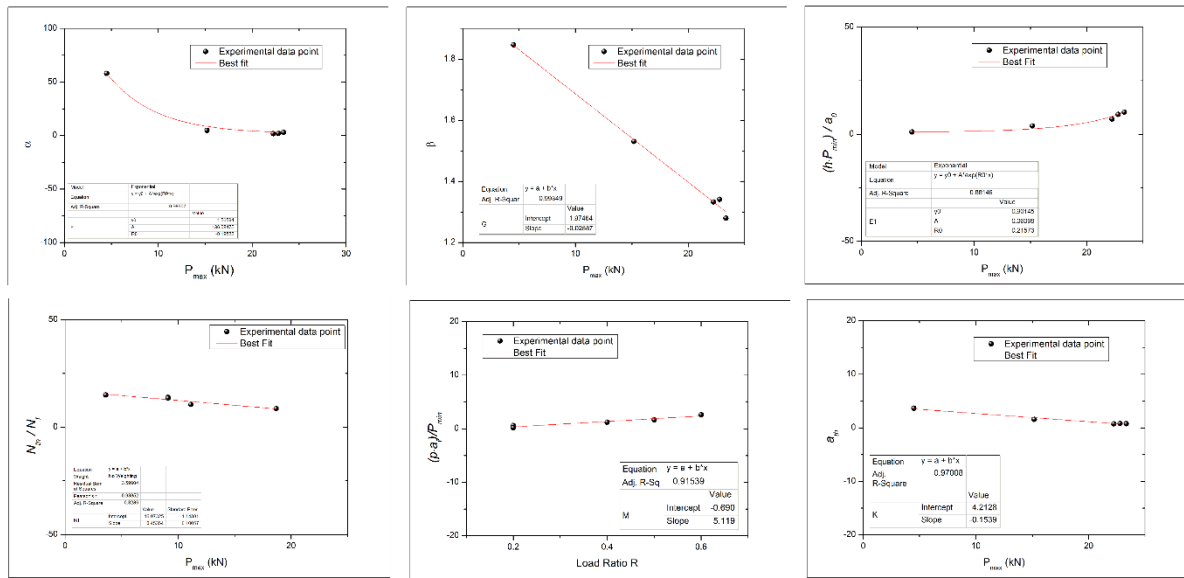


Fig. 8 - Best fit of the model parameters values in function of loading conditions.

In particular, for h , N_{th} and p three different expressions have been introduced:

$$C_1 = \frac{h P_{min}}{a_0} \quad (8)$$

$$C_2 = \frac{N_{th}}{N_0} \quad (9)$$

$$C_3 = \frac{p a_f}{P_{min}} \quad (10)$$

Expression reported as Eqns. (8) and (10) have shown to be related to the maximum applied load, as shown in Fig. 8. Eq. (9) is related to the load ratio and it is shown in Fig. 8. In terms of the quality of fit, it can be assessed with the value of the coefficient of correlation (R^2). A good fitting is achieved if the coefficient of correlation is between 0.8 and 1 for all the correlations identified [54]. The N_{th} in function of P_{max} , as shown in Fig. 8 has the

lower coefficient of determination of 0.8286 in current study. This value is however still within the acceptable range and the correlation between the considered parameters values is acceptable.

The extrapolation of the curves as shown in Fig. 5 reaches $N = -N_{th}$ asymptotically, which can be used to generate ΔK_{th} values based on the theory of identifying threshold [19, 21]. The range between the maximum and minimum values of the predicted ΔK_{th} for each dataset is quite small so that the average value of the threshold is used. The reference values for materials considered in this paper have been taken from literature in order to verify the model. In the literature a range of threshold values are also mentioned for a particular material for a constant R [18, 41, 55]. Fig. 10 shows the comparison between the threshold values obtained using the model and threshold values found in the literature for the same kind of material. The values considered as literature values are based on ESDU documents [41] for aluminium alloy 7075-T6 (at $R = 0.4, 0.5$ and 0.6) and aluminium alloy 2024-T3 (at $R = 0.2$). For 2024-T351 (at $R = 0.2$) the literature value is taken based on ΔK_{th} value provided by [44] and normalized threshold SIF range against R curve provided by [43]. The average threshold value of the model is used for the comparison. In Ghonem (set I-III), Vilker, Wu and Ni datasets, the threshold values of the corresponding materials from the literature are $1.5 \text{ MPa}\sqrt{\text{m}}$, $1.7 \text{ MPa}\sqrt{\text{m}}$, $1.9 \text{ MPa}\sqrt{\text{m}}$, $2.85 \text{ MPa}\sqrt{\text{m}}$ and $3.6 \text{ MPa}\sqrt{\text{m}}$. Comparing these values with those predicted by the proposed model, the percentages of error are approximately 5.3%, 4.1%, 0%, 2.1% and 0.3%, respectively.

As shown earlier in Fig. 6, in all cases there is a band of threshold values predicted for the same material with the literatures showing the same trends. The threshold vs R graph provided by [41] shows a small range of threshold values with upper and lower limit indicated for 2024-T3 aluminium alloy. Different investigations by Newman and Raschau [1, 2, 28-30] also found a range of threshold based on different experimental methods used e.g. load reduction (LR) methods, K_{max} constant methods and far-field cyclic compression methods.

Recently, Molent. et al [18] used a FCG threshold parameter ΔK_{thr} to explain the scatter in the fatigue life prediction. The ΔK_{thr} is used to explain the dependency of the threshold values on the material properties, R ratio, crack length and loading method used for the testing phase. From literature [45, 56], it was found that $\Delta K_{thr} = 0$ produces conservative crack growth predictions for different aluminium alloys. The fact that different values of the threshold SIF were reported for the same material in literature can be treated as supporting evidence to the concept of cyclic stress intensity threshold. For the material used in generating Virkler dataset a

range of ΔK_{thr} ($2.9 \div 4.2 \text{ MPa}\sqrt{\text{m}}$) it is reported whilst the material related to Wu and Ni dataset a range of ΔK_{thr} ($0 \div 4.2 \text{ MPa}\sqrt{\text{m}}$). Moreover, for 7075-T6 aluminium alloy material at a $R = -1$ range of ΔK_{thr} ($0.6 \div 1.13 \text{ MPa}\sqrt{\text{m}}$) was found. In other published papers [55] it has been shown a threshold band ΔK_{thr} ($2.8 \div 4 \text{ MPa}\sqrt{\text{m}}$) at $R = 0.33$ for 2024-T351 aluminium alloy. All these values are in good agreement with those estimated by the proposed model.

In order to investigate the variability of the threshold SIF range, the response surface reporting the correlation of this latter parameter as functions of the maximum applied load and the load ratio is shown in Fig. 9. The values shown in the graph related to the threshold SIF are those identified through the fitting analysis of the raw data. Although all the values identified in the analysis related to different aluminium alloys are shown on the same plot, the validity of the contour plot is limited to the R and P_{max} ranges investigated in this paper and the alloys considered in the tests are referring to the datasets used for the analysis. However, the contour can represent a valid tool for a preliminary identification of the threshold SIF range.

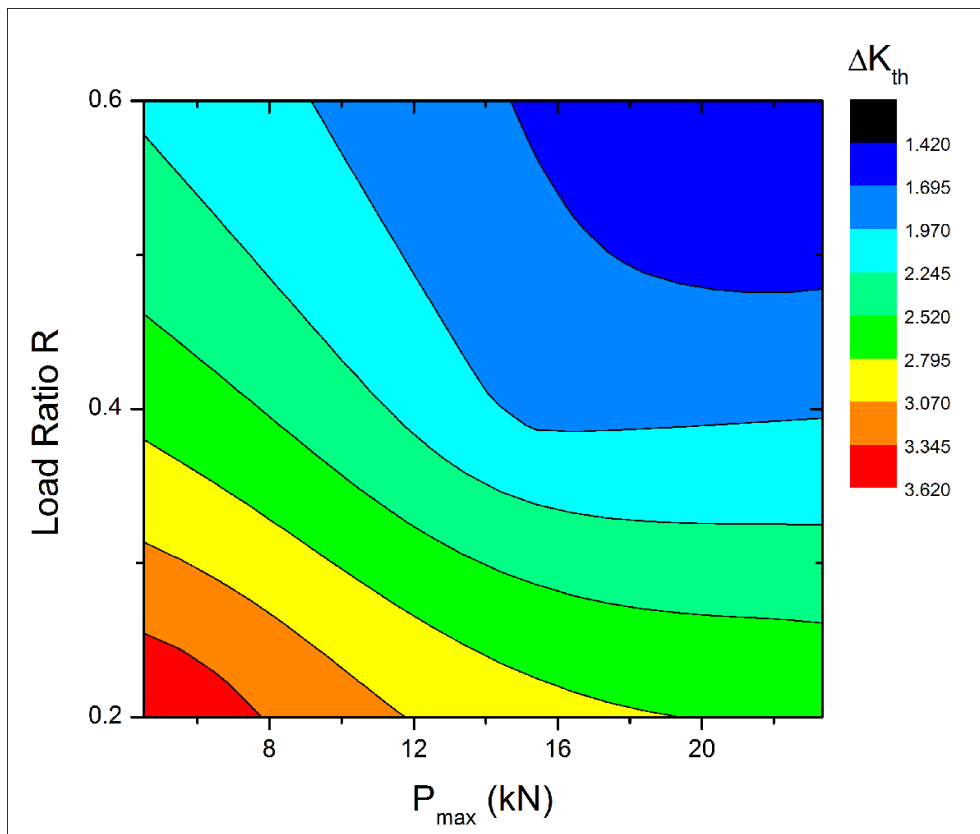


Fig. 9 - Contour plot of the ΔK_{th} in function of the maximum applied load and the load ratio.

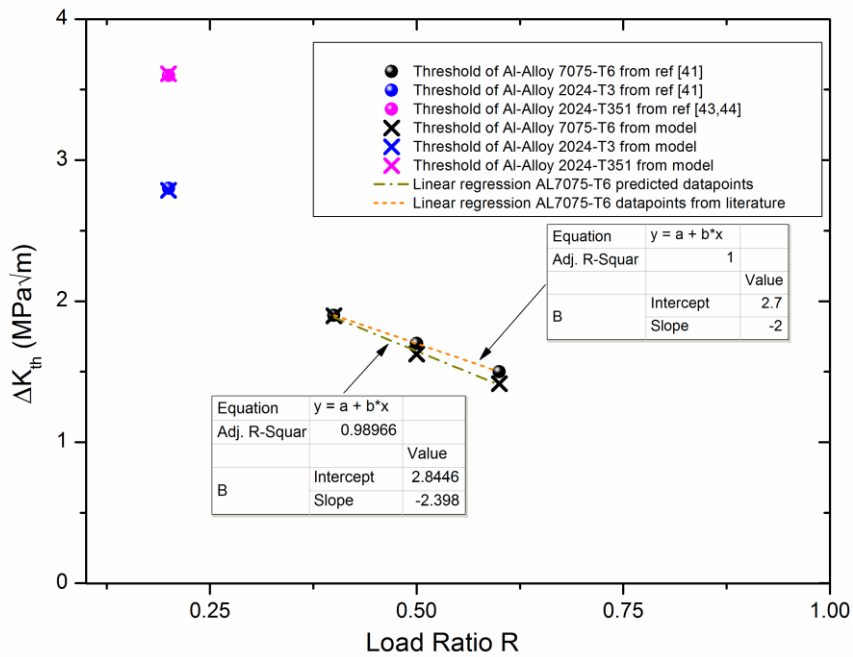


Fig. 10 threshold vs load ratio data where thresholds of model and literature are compared

Reporting all the results on the same graph in Fig. 10, it is possible to identify common trend useful to compare the results with the literature values. Firstly, the threshold line found with declined linear pattern or shape in relation to R for the 7075-T6 aluminium alloy is qualitatively and quantitatively consistent with the line found in the literature [41]. The percentage of error ranges between 0.24% and 5.61%, which is quite low considering the scattering nature of the fatigue test data. They should converge at the higher value of R but it was found that the scatter was getting bigger and reached 5.61% at $R = 0.6$. This difference or scatter could be explained by different experimental methods used and the corresponding crack closure effects as referred by [1, 2, 28-30]. All the predicted threshold values of aluminium alloys (7075-T6 and 2024-T6) underestimate the values from literature (see for example [41]) except for the threshold value of 2024-T351 aluminium alloy which overestimates the literature value from [43, 44]. For 7076-T6 aluminium alloy, the threshold values from literature [3] at $R = 0.2$ is $2.3 \text{ MPa}\sqrt{\text{m}}$ whilst the value derived using the analytical model here proposed is equal to $2.3651 \text{ MPa}\sqrt{\text{m}}$ with an error less than 3%.

In general, the yield strength of 7075-T6, 2024-T3 and 2024-T351 aluminium alloys are 510 MPa, 350 MPa and 330 MPa, respectively. The threshold values found from the model for the three alloys at $R = 0.2$ are $3.6 \text{ MPa}\sqrt{\text{m}}$, $2.8 \text{ MPa}\sqrt{\text{m}}$ and $2.4 \text{ MPa}\sqrt{\text{m}}$ respectively. This indicates a correlation between the yield strength

and threshold of these aluminium alloys: higher strength aluminium alloy possesses relatively higher threshold and vice versa. This supports the statement of the previous investigations which found the same type of correlation between the strength and threshold of materials [19, 36, 37].

It should be added that, the values of the a_{th} in Eq. (6) were found to influence the threshold value since it is the value of the crack length corresponding to the fatigue life value equal to $N = -N_{th}$. Therefore, a_{th} values can be further considered to correlate with the material properties, the load ratio as well as the geometry of the cracked component. It is possible to find in literature that the threshold value increases with the strength of the material [19, 36, 37]. Further research should be carried out to properly address this correlation, which could help in both identifying the parameter values and giving them a more physical understanding.

Conclusions

An analytical model for the interpolation of crack propagation data has been developed. The threshold SIF range has been derived for different materials and different specimen geometries. The new model has been shown to fit, with the needed accuracy, to a wide range of experimental data produced with different specimen geometries, different materials and different loading conditions. Moreover, it has been highlighted that it is possible to identify, by means of the above model, the value of the threshold SIF range with an error, as compared to the values reported in literature, of less than 6%. The relation between ΔK_{th} and R ratio predicted by the model agrees well with the literature results. The proposed model can therefore be valuable in identifying the threshold of stress intensity factor range for fatigue crack growth.

Conflict of Interests

The authors declare that there is no conflict of interests regarding the publication of this paper.

References

1. Newman, J., et al., *Compression pre-cracking to generate near threshold fatigue-crack-growth rates in two aluminum alloys*. International journal of fatigue, 2005. **27**(10): p. 1432-1440.
2. Newman Jr, J., J. Ruschau, and M. Hill, *Improved test method for very low fatigue-crack-growth-rate data*. Fatigue & Fracture of Engineering Materials & Structures, 2011. **34**(4): p. 270-279.
3. Klesnil, M. and P. Lukáš, *Influence of strength and stress history on growth and stabilisation of fatigue cracks*. Engineering Fracture Mechanics, 1972. **4**(1): p. 77-92.

4. Collipriest Jr, J., *An experimentalist's view of the surface flaw problem*. Paper from "The Surface Crack- Physical Problems and Computational Solutions", ASME, New York. 1972, 43-61., 1972.
5. McEvily, A., *Phenomenological and microstructural aspects of fatigue*. The microstructure and design of alloys, 1973: p. 204-225.
6. Johnson, W., *Multi-parameter yield zone model for predicting spectrum crack growth*, in *Methods and Models for Predicting Fatigue Crack Growth Under Random Loading*. 1981, ASTM International.
7. Chang, J., *Round-robin crack growth predictions on center-cracked tension specimens under random spectrum loading*, in *Methods and Models for Predicting Fatigue Crack Growth Under Random Loading*. 1981, ASTM International.
8. Newman, J., *Prediction of fatigue crack growth under variable-amplitude and spectrum loading using a closure model*, in *Design of Fatigue and Fracture Resistant Structures*. 1982, ASTM International.
9. Xiulin, Z. and M.A. Hirt, *Fatigue crack propagation in steels*. Engineering Fracture Mechanics, 1983. **18**(5): p. 965-973.
10. Forman, R.G. and S.R. Mettu, *Behavior of surface and corner cracks subjected to tensile and bending loads in Ti-6Al-4V alloy*. 1990.
11. Huang, X. and T. Moan, *Improved modeling of the effect of R-ratio on crack growth rate*. International Journal of Fatigue, 2007. **29**(4): p. 591-602.
12. Harter, J.A., *AFGROW users guide and technical manual*. 1999, DTIC Document.
13. Newman Jr, J.C., *FASTRAN-2: A fatigue crack growth structural analysis program*. NASA STI/Recon Technical Report N, 1992. **92**: p. 30964.
14. Hu, W. and K. Walker. *Fatigue crack growth from a notch under severe overload and underload*. in *The International Conference on Structural Integrity and Failure*. 2006.
15. Castillo, E., A. Fernández-Canteli, and D. Siegele, *Obtaining S-N curves from crack growth curves: an alternative to self-similarity*. International Journal of Fracture, 2014. **187**(1): p. 159-172.
16. Beden, S., S. Abdullah, and A. Ariffin, *Review of fatigue crack propagation models for metallic components*. European Journal of Scientific Research, 2009. **28**(3): p. 364-397.
17. Hartman, A. and J. Schijve, *The effects of environment and load frequency on the crack propagation law for macro fatigue crack growth in aluminium alloys*. Engineering Fracture Mechanics, 1970. **1**(4): p. 615-631.
18. Molent, L. and R. Jones, *The influence of cyclic stress intensity threshold on fatigue life scatter*. International Journal of Fatigue, 2016. **82, Part 3**: p. 748-756.
19. Zerbst, U., et al., *About the fatigue crack propagation threshold of metals as a design criterion—A review*. Engineering Fracture Mechanics, 2016. **153**: p. 190-243.
20. Suresh, S. and R.O. Ritchie, *Propagation of short fatigue cracks*. International Metals Reviews, 1984. **29**(1): p. 445-475.
21. Anderson, T.L., *Fracture mechanics: fundamentals and applications*. 2005: CRC press.
22. Paris, P. and F. Erdogan, *A critical analysis of crack propagation laws*. Journal of basic engineering, 1963. **85**(4): p. 528-533.
23. Pearson, S., *Initiation of fatigue cracks in commercial aluminium alloys and the subsequent propagation of very short cracks*. Engineering Fracture Mechanics, 1975. **7**(2): p. 235-247.
24. International, A., *Standard Test Method for Measurement of Fatigue Crack Growth Rates*. 2011: ASTM International.
25. Hudak Jr, S., et al., *Development of standard methods of testing and analyzing fatigue crack growth rate data*. 1978, DTIC Document.
26. Vormwald, U.D.-I.M., *Elastic-Plastic Fatigue Crack Growth*, in *Advanced Methods of Fatigue Assessment*. 2013, Springer. p. 391-481.

27. ISO, B., 12108, 2002: 'Metallic materials-Fatigue testing-Fatigue crack growth method'. British Standards Institution, London.
28. Ruschau, J. and J. Newman. *Compression precracking to generate near threshold fatigue crack growth rates in an aluminum and titanium alloy*. in *Seventh International ASTM/ ESIS Symposium on Fatigue and Fracture Mechanics (36th ASTM National Symposium on Fatigue and Fracture Mechanics)*. 2009. ASTM International.
29. Newman Jr, J.C. and Y. Yamada, *Compression precracking methods to generate near-threshold fatigue-crack-growth-rate data*. *International Journal of Fatigue*, 2010. **32**(6): p. 879-885.
30. Forth, S.C., J.C. Newman, and R.G. Forman, *On generating fatigue crack growth thresholds*. *International Journal of Fatigue*, 2003. **25**(1): p. 9-15.
31. Pippin, R., *Threshold and effective threshold of fatigue crack propagation in ARMCO iron I: The influence of grain size and cold working*. *Materials Science and Engineering: A*, 1991. **138**(1): p. 1-13.
32. Suresh, S., G. Zamiski, and D.R. Ritchie, *Oxide-induced crack closure: an explanation for near-threshold corrosion fatigue crack growth behavior*. *Metallurgical Transactions A*, 1981. **12**(8): p. 1435-1443.
33. Newman, J., *Fatigue and Crack-growth Analyses under Giga-cycle Loading on Aluminum Alloys*. *Procedia Engineering*, 2015. **101**: p. 339-346.
34. Li, B. and L. Rosa, *Prediction models of intrinsic fatigue threshold in metal alloys examined by experimental data*. *International Journal of Fatigue*, 2016. **82**: p. 616-623.
35. Chowdhury, P.B., H. Sehitoglu, and R.G. Rateick, *Predicting fatigue resistance of nano-twinned materials: Part II—Effective threshold stress intensity factor range*. *International Journal of Fatigue*, 2014. **68**: p. 292-301.
36. Wasen, J. and E. Heier, *Fatigue crack growth thresholds—the influence of Young's modulus and fracture surface roughness*. *International journal of fatigue*, 1998. **20**(10): p. 737-742.
37. Pippin, R. and P. Weinert, *The effective threshold of fatigue crack propagation in aluminium alloys. II. The influence of particle reinforcement*. *Philosophical Magazine A*, 1998. **77**(4): p. 875-886.
38. Varfolomeev, I., M. Luke, and M. Burdack, *Effect of specimen geometry on fatigue crack growth rates for the railway axle material EA4T*. *Engineering Fracture Mechanics*, 2011. **78**(5): p. 742-753.
39. Regazzi, D., et al., *Experimental and numerical investigations of fatigue crack closure in standard specimens*. *DVM-AK Bruchvorgänge, DVM-Bericht*, 2013. **245**: p. 157-166.
40. Hutař, P., et al. *Fatigue Crack Propagation Rate in EUROFER 97 Estimated Using Small Specimens*. in *Key Engineering Materials*. 2011. Trans Tech Publ.
41. Hookham, C.R., *Fatigue crack propagation rates and threshold stress intensity factor ranges for aluminium alloy sheet.*, in *ESDU Fatigue - Fracture Mechanics Series*. 2000-03. p. 1-32.
42. Boyce, B. and R. Ritchie, *Effect of load ratio and maximum stress intensity on the fatigue threshold in Ti-6Al-4V*. *Engineering Fracture Mechanics*, 2001. **68**(2): p. 129-147.
43. Kwofie, S., *Equivalent stress approach to predicting the effect of stress ratio on fatigue threshold stress intensity range*. *International Journal of Fatigue*, 2004. **26**(3): p. 299-303.
44. Jones, R., L. Molent, and K. Walker, *Fatigue crack growth in a diverse range of materials*. *International Journal of Fatigue*, 2012. **40**: p. 43-50.
45. Wu, X.-R., et al., *Small crack growth and fatigue life predictions for high-strength aluminium alloys: Part I: Experimental and fracture mechanics analysis*. *Fatigue & fracture of engineering materials & structures*, 1998. **21**(11): p. 1289-1306.
46. De Iorio, A., et al., *A three-parameter model for fatigue crack growth data analysis*. *Frattura ed Integrità Strutturale*, 2012(21): p. 21-29.
47. Ghonem, H. and S. Dore, *Experimental study of the constant-probability crack growth curves under constant amplitude loading*. *Engineering Fracture Mechanics*, 1987. **27**(1): p. 1-25.

48. Virkler, D., B. Hillberry, and P. Goel, *The statistical nature of fatigue crack propagation*. Journal of Engineering Materials and Technology, 1979. **101**(2): p. 148-153.
49. Wu, W. and C. Ni, *Statistical aspects of some fatigue crack growth data*. Engineering Fracture Mechanics, 2007. **74**(18): p. 2952-2963.
50. Barter, S., et al., *An experimental evaluation of fatigue crack growth*. Engineering failure analysis, 2005. **12**(1): p. 99-128.
51. Frost, N. and D. Dugdale, *The propagation of fatigue cracks in sheet specimens*. Journal of the Mechanics and Physics of Solids, 1958. **6**(2): p. 92-110.
52. Mohanty, J., B. Verma, and P. Ray, *Determination of fatigue crack growth rate from experimental data: a new approach*. International Journal of Microstructure and Materials Properties, 2010. **5**(1): p. 79-87.
53. Grasso, M., et al., *A four-parameters model for fatigue crack growth data analysis*. Frattura ed Integrità Strutturale, 2013(26): p. 69.
54. Nagelkerke, N.J., *A note on a general definition of the coefficient of determination*. Biometrika, 1991. **78**(3): p. 691-692.
55. *Alloy 2024 sheet and plate, excellent fatigue properties—consistent performance*. Alcoa mill products, Inc.: Alcoa mill products, Inc. P.O. Box 8025 ,Bettendorf, IOWA 52722, www.millproducts-alcoa.com. p. 523-9596
56. Newman, J., et al., *Small-crack growth and fatigue life predictions for high-strength aluminium alloys. Part II: crack closure and fatigue analyses*. Fatigue and Fracture of Engineering Materials and Structures, 2000. **23**(1): p. 59-72.